Isolation and characterization of a californium metallocene

DOI:
10.1038/s41586-021-04027-8

Document Version
Accepted author manuscript

Isolation and Characterization of a Californium Metallocene

Conrad A. P. Goodwin,[†[a]] Jing Su,[†[b,c]] Lauren M. Stevens,[[a]] Frankie D. White,[[a]] Nickolas H. Anderson,[[a]] John D. Auxier II,[[a]] Thomas E. Albrecht-Schönzart,[[d]] Enrique R. Batista,*[[b]] Sasha F. Briscoe,[[e]] Justin N. Cross,[[a]] William J. Evans,*[[f]] Alyssa N. Gaiser,[[d]] Andrew J. Gaunt,*[[a]] Michael R. James,[[a]] Michael T. Janicke,[[a]] Tener F. Jenkins,[[f]] Zachary R. Jones,[[a]] Stosh A. Kozimor,*[[a]] Brian L. Scott,[[g]] Joseph. M. Sperling,[[d]] Justin C. Wedal,[[f]] Cory J. Windorff,[[d]] Ping Yang,*[[b]] and Joseph W. Ziller[[f]]

[a] Chemistry Division, Los Alamos National Laboratory, Los Alamos, NM 87545 (USA)

[b] Theoretical Division, Los Alamos National Laboratory, Los Alamos, NM 87545 (USA)

[c] College of Chemistry, Sichuan University, Chengdu 610064 (China)

[d] Department of Chemistry and Biochemistry, Florida State University, 95 Chieftain Way, Tallahassee, FL 32306 (USA)

[e] Radiation Protection Division, Los Alamos National Laboratory, Los Alamos, NM 87545 (USA)

[f] Department of Chemistry, University of California, Irvine, CA 92697 (USA)

[g] Materials Physics & Applications Division, Los Alamos National Laboratory, Los Alamos, NM 87545 (USA)

* Correspondence to: erb@lanl.gov; wevans@uci.edu; gaunt@lanl.gov; stosh@lanl.gov; pyang@lanl.gov.

† These authors contributed equally to this work.

Summary

Californium (Cf) is currently the heaviest element accessible above microgram quantities. Cf isotopes impose severe experimental challenges due to their scarcity and radiological hazards. Consequently, chemical secrets ranging from the accessibility of 5f / 6d valence orbitals to engage in bonding, the role of spin-orbit coupling in electronic structure, and reactivity patterns compared to other f-elements, remain locked. Organometallic molecules were foundational in elucidating periodicity and bonding trends across the periodic table,[1-3] with a 21st century renaissance of organometallic thorium (Th) through plutonium (Pu) chemistry[4-12], and to a smaller extent americium (Am)[13], transforming chemical understanding. Yet, analogous curium (Cm) – Cf chemistry has lain dormant since the 1970s. Here, we revive air-/moisture-sensitive Cf chemistry through the synthesis and characterization of $[Cf(C_5Me_4H)_2Cl_2K(OEt_2)]_n$ from two milligrams of ^{249}Cf. This bent metallocene motif, not previously structurally authenticated beyond uranium (U)[14,15], contains the first crystallographically characterized Cf–C bond. Analysis suggests the Cf–C bond is largely ionic with a small covalent contribution. Lowered Cf 5f orbital energy *vs.* Dy 4f in the colourless, isoelectronic, and isostructural $[Dy(C_5Me_4H)_2Cl_2K(OEt_2)]_n$ results in an orange Cf compound, contrasting with light green typically associated with Cf compounds[16-22].

Main

The first actinide (An) metallocene, uranocene, $[U(C_8H_8)_2]$, reported in 1968[2,23], featured two aromatic $(C_8H_8)^{2-}$ rings sandwiching the U^{4+} ion and demonstrated that non-actinyl molecules are capable bonding that is intermediate between covalent transition metals and ionic lanthanide ions[24]. Recent organometallic and non-aqueous Th and U chemistry has exploded[12], redrawing the boundaries of known oxidation states[25], multiply-bonded molecular motifs[26], small molecule reactivity[4], and covalency/electronic structure trends[5,8,24,27]. Analogous advances with the heaviest available transuranium actinides are limited, although there are some, such as the deep red putative $CfCp_3$, that contrasted with the light green of most other Cf compounds[22]. While several $AnCp_3$ (An = Th, U – Cf)[6,9,22,28,29] molecules have been synthesized and/or examined by theory[30,31], none have been authenticated beyond Pu[6,9,11]. Related bent Th and U metallocenes like $[M(C_5R_5)_2X_n]$ (X = anion; n = 1, 2) have played a major role in improving our understanding of actinide electronic structure and

bonding[32,33] but this motif remains structurally unverified beyond U[14,15]. The first structurally authenticated An–C bonds for Pu appeared in 2017[7,10], and in 2019 for Am[13] in [Am(Cp^{tet})$_3$] (Cp^{tet} = {C_5Me_4H}). Advancement beyond Am represents another step-change in difficulty; we tackle that challenge here through the isolation and characterization of an organocalifornium metallocene.

Results and discussion

Synthesis. In targeting an organocalifornium complex we had to account for: 1) availability and radiation hazards from ^{249}Cf limiting reaction scale to 2 mg of $^{249}Cf^{3+}$; and, 2) the handful of Cf single-crystal X-ray diffraction studies[16-18,21,34-37] suggest radiolytic degradation of crystals is minimised by employing short timescales,[18,22] which would also reduce unknown radiolytic impacts on organometallic reaction pathways. Thus, a one-day reaction protocol was developed based on lanthanide surrogates. A Cf^{3+}-chloride solution in $HCl_{(aq)}$, containing 2 mg of $^{249}Cf^{3+}$, was converted to mint-green anhydrous '$CfCl_3(DME)_n$', then treated with KCp^{tet} (3.5 equiv.) in Et_2O at room temperature (Fig. 1a). The reaction mixture progressively changed from salmon-orange to red-orange (*c.f.* ruby red $Cf(Cp)_3$)[22] to yellow. Workup afforded dark orange columnar crystals (Supplementary Figs. 17 – 18). Single crystal X-ray diffraction from three crystals showed all were $[Cf(Cp^{tet})_2Cl_2K(OEt_2)]_n$ (**2-Cf**, Fig. 1b). See Supplementary Information for experimental details.

Fig. 1. Synthesis and solid-state structure of 2-Cf

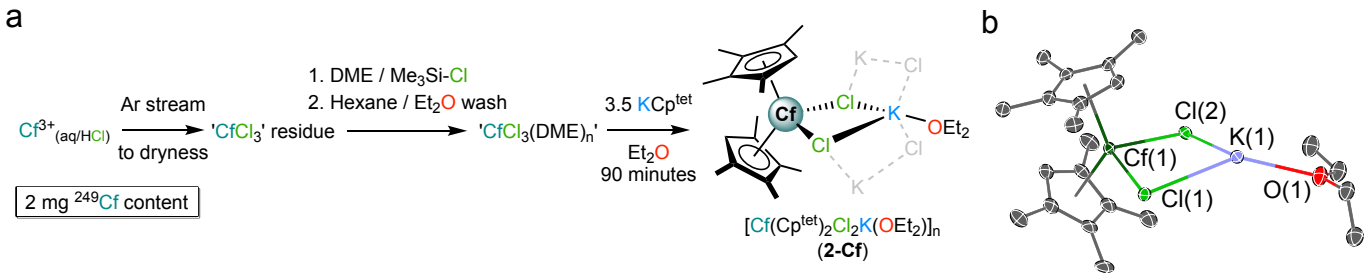

a, the synthesis of **2-Cf** from aqueous acidic media using 2 mg of ^{249}Cf. **b**, the solid-state structure of the monomeric unit about Cf(1) with selective atom labelling (Cf, dark green; K, lavender; Cl, light green; O, red; C, grey).

Comparing Californium and Lanthanide Reactivities. Consider the reactivity of lanthanides that are either larger (6-coordinate radii given; Sm^{3+}, 0.958 Å), similar in size (Eu^{3+}, 0.947 Å; and Gd^{3+}, 0.938 Å), or smaller (Dy^{3+}, 0.912 Å; and Ho^{3+}, 0.901 Å) than Cf^{3+} (0.95 Å)[38]. Reactions between KCp^{tet} and '$SmCl_3(DME)_n$' in Et_2O readily produced $[Sm(Cp^{tet})_3]$, **1-Sm**[39], not the Sm analogue of **2-Cf**. Room temperature conditions allowed isolation of $[Ln(Cp^{tet})_2Cl_2K(OEt_2)]_n$ (Ln = Gd, **2-Gd**; Dy, **2-Dy**), but **1-Gd** was only isolable when reactions were heated to 70 °C, while **1-Dy**[40] and **1-Ho** required multi-day reaction protocols. The closest size match for Cf^{3+}, Eu^{3+}, was precluded from comparison as the Eu^{2+} complex, $[Eu(Cp^{tet})_2(THF)_2]$ (**3**), was the only identifiable product. Although the behavior of Cf^{3+} might not be dictated by its ionic radius, reactions with metals larger (Sm^{3+}) and smaller (Gd^{3+}) than Cf^{3+} both afforded **1-Sm** and **2-Gd** using short timescales. Therefore, it was reasonable to consider that either **1-Cf** or **2-Cf** could be generated and isolated on a small-scale with short reaction times. When a second reaction of '$CfCl_3(DME)_n$' with KCp^{tet} in Et_2O at 70 °C (analogously to **1-Gd**) was performed, we observed the same series of colour changes as the synthesis of **2-Cf** but the only crystalline material isolated was $[K(OEt_2)(Cp^{tet})]_n$ (**4**). Extended Data Fig 1 summarizes syntheses.

To consider effects from radiolysis on the formation of **2-Cf**, we repeated the reported synthesis of **1-^{243}Am**[13], using ^{241}Am ($t_{1/2}$ = 432.6 years, 5.638 MeV α-emission), which has a similar decay rate and α-particle energies to ^{249}Cf ($t_{1/2}$ = 351 years, 6.295 MeV α-emission). This comparison allows direct evaluation of increased decay-rate of ^{241}Am relative to ^{243}Am ($t_{1/2}$ = 7,364 years, 5.438 MeV α-emission, principal γ-line 74.66 KeV). Crystals of **1-^{241}Am** were isolated in good yield and definitively characterized (Supplementary Figs. 9, 22, 29 – 32). These data are consistent with neither an enhanced rate of α-emission, nor 59.54 KeV γ-emission, having a notable effect upon the formation of **1-Am**, and may suggest that the α-emission from ^{249}Cf is not a major contributor in the isolation of **2-Cf** *vs* **1-Cf**. However, we cannot discount effects of the higher energy γ-emissions from ^{249}Cf compared to ^{241}Am (388.16 and 59.54 KeV. respectively). Other possibilities are that **2-Cf** and **4** crystallize preferentially from a mixture of **1-Cf/2-Cf**, or that **2-Cf** is a kinetic product of the short reaction times employed to minimize radiolytic effects, and that multi-day syntheses (like **1-Ho**) are required to access **1-Cf**.

Structural characterisation. Complex **2-Cf** crystallized in the orthorhombic space group P*ca*2$_1$ with two {Cf(Cp^{tet})$_2$Cl$_2$K(OEt$_2$)} molecules in the asymmetric unit (Extended Data Fig. 2). While Cf(1) is described as *trans*, the rings on Cf(2) exhibit disorder and half the occupancy comprises a somewhat *cis* configuration. The calculated energy difference between *cis* and *trans* forms of **2-Cf** ($\Delta E_{cis/trans}$ = 1.1 kcal/mol) is small and consistent with the co-existence of the two conformations. Both **2-Ln** (Ln = Gd, Dy) complexes are isomorphous (P*ca*2$_1$) to **2-Cf** but with all-*trans* configurations. A polymorph (P*bca*) of **2-Gd** was found with a single *cis* molecule in the asymmetric unit; both forms come from a single batch of crystals ($\Delta E_{cis/trans}$ = 0.88 / 0.93 kcal/mol for Gd / Dy respectively).

The Cf atoms in **2-Cf** are *pseudo*-tetrahedral – the coordination sphere is comprised of two chlorides and two η^5-Cp^{tet} ligands (Cf(1)–C$_{Cp}$ range: 2.623(12) – 2.718(13) Å). The structure is comparable to **2-Ln** (Ln–C$_{Cp}$: Ln = Gd, 2.620(12) – 2.722(14) Å; Dy, 2.583(8) – 2.737(11) Å) once differences in ionic radii are considered[38]. The Cf–Cl distances (range: 2.653(4) – 2.670(6) Å) and Cl–Cf–Cl angles (89.84(14)° and 89.98(14)°) are tightly bunched, as are the Cp$^{tet}_{centroid}$···Cf···Cp$^{tet}_{centroid}$ angles (Cf(1), 130.99(3)°; Cf(2), 130.51(3)°). Few other Cf–Cl bonds have been structurally characterised, but in CfCl$_3$[21] they span a wide range (2.690(7) – 2.940(6) Å), and are generally longer than **2-Cf**. The M–Cl lengths in nine-coordinate M$_4$[B$_{16}$O$_{26}$(OH)$_4$(H$_2$O)$_3$Cl$_4$][35] (M = Cf, avg. 2.762(10) Å; Gd, avg. 2.815(2) Å) are longer than those in **2-Cf**, and show a larger Cf *vs* Gd difference than observed in **2-M**.

UV-vis-NIR spectroscopy. Dark orange **2-Cf** (5f^9) contrasts with most other mint-green Cf^{3+} complexes[16,18-20,34,37], and colourless **2-Dy** (4f^9). A UV-vis-NIR spectrum of **2-Dy** exhibits no absorptions from *ca*. 40,000 to 7,100 cm^{-1}, whereas **2-Cf** exhibits an intense ligand to metal charge-transfer (LMCT) tail that dominates from 18,000 cm^{-1} (556 nm) to at least 28,570 cm^{-1} (350 nm) (Fig. 2a-b), and broad Laporte-forbidden 5f→5f transitions between 6,800 – 18,000 cm^{-1} (1,470 – 556 nm). The solid-state UV-vis-NIR spectrum of **2-Cf** (Fig. 2a black and red lines) has superficial similarities with aqueous Cf^{3+} (Fig. 2a, blue dotted line) and single crystals of anhydrous CfCl$_3$[19], though several differences are noted below. The low energy region (< 18,000 cm^{-1}, Fig. 2b) shows five bands whose centres align well with the lowest energy bands of CfCl$_3$: A (^{6}F$_{9/2}$), B, C (^{6}F$_{3/2}$), D, and E (^{6}H$_{15/2}$)[20], where the terms in parenthesis describe the largest component of the excited

state. The nephelauxetic effect relates the Racah *B* parameter (inter-electronic repulsion) in a complex to that of a free metal ion. A reduction of *B* upon complexation usually lowers the energy of electronic excitations (e.g. 5f→5f), though for metals with pronounced spin orbit coupling (such as actinides), it can shift peaks to both higher- or lower-energy[19]. This reduction in *B* can occur from orbital expansion through covalency because the molecular orbitals are more diffuse or from charge transfer. Regardless of the mechanism, when comparing **2-Cf** to aqueous Cf^{3+} or $CfCl_3$ we see modest (*ca.* 100 cm^{-1}) shifts for most of the bands that are suggestive of Cf–ligand covalency and/or charge-transfer effects.

Fig. 2. UV-vis-NIR spectra of 2-Cf.

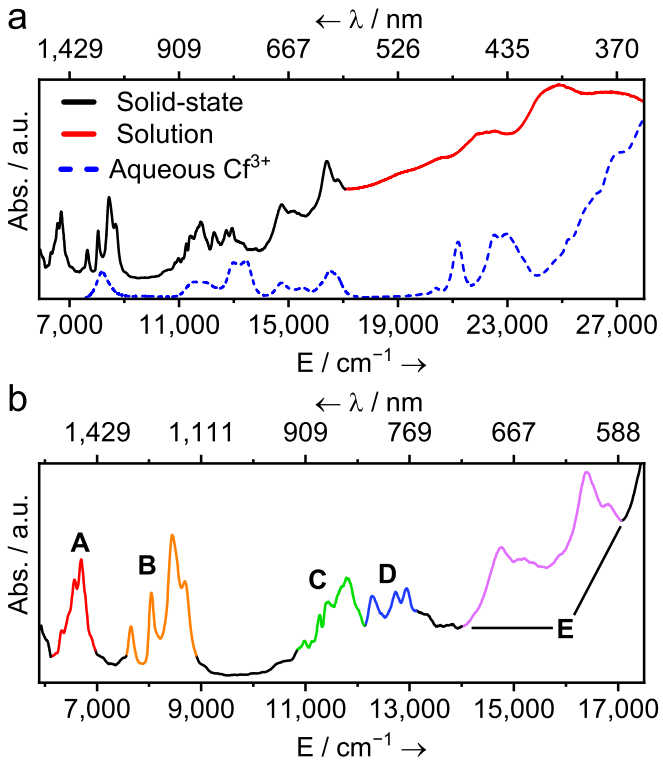

a, Truncated solid-state (black line, 5,890 – 17,100 cm^{-1}; 1,698 – 585 nm) and solution (red line, 17,100 – 28,000 cm^{-1}; 585 – 357 nm) spectra of **2-Cf**; and the solution spectrum of the Cf^{3+} ion in 2 M aqueous HCl (blue dotted line, 7,550 – 28,000 cm^{-1}; 1,325 – 357 nm). A combination of both is shown as the solid-state spectrum is clearer in the low energy region, but is saturated above 17,000 cm^{-1}. **b**, The solid-state spectrum between 5,890 – 18,000 cm^{-1} (1,698 – 556 nm), showing 5f→5f transitions that are isolated from the LMCT region. A (red), B (orange), C (green), D (blue), and E (purple) correspond to line groups in the spectrum of $CfCl_3$[19,20].

Electronic Structure Calculations. To construct a full bonding picture in **2-Cf** *vs* **2-Dy** we have examined molecular orbital (MO) energy level and composition, Mulliken population, bond order analysis, and QTAIM (quantum theory of atoms in molecules) analysis (Extended Data Tables 1-3). In **2-Cf** there is consistently an increased Cf 5f contribution to the MOs compared to Dy 4f contributions in **2-Dy** (Extended Data Fig. 3). Charge population and QTAIM assessment of both complexes shows largely polar ionic bonding similar to $[An(Cp)_3]$ complexes[30]. These techniques are less sensitive to the small but notable differences seen by comparing MO energy levels which show increased metal-ligand orbital mixing in **2-Cf** compared to **2-Dy**. The bonding interactions between Cf–C and Cf–Cl are depicted in Supplementary Figure S75.

Simulation of UV-vis-NIR spectra. Simulated UV-vis-NIR spectra of the **2-M** series (M = Cf, Gd, Dy) using complete active space self-consistent field (CASSCF) including spin-orbit (SO) and perturbative correlation corrections (SO-CASSCF/NEVPT2) relate theoretical results with experimental spectroscopic features. To balance accuracy and computational cost, the active space [9e,7o] simulated low energy (< 18,000 cm^{-1}) 5f→5f transitions **2-Cf** (Fig. 3, black dashed line), while a larger active space [17e, 11o] which included ligand orbitals captured the higher energy (> 18,000 cm^{-1}) ligand→5f transitions (Fig. 3, black solid line). Calculated features (Fig. 3, red solid and dashed lines, a′ – k′ and l″ – s″) excellently reproduce the experimental spectrum (Supplementary Tables 10 – 12). The orientation of the Cp^{tet} ring has negligible impact on 5f→5f electronic absorption spectra (Supplementary Figs. 63 – 64).

Fig. 3. Experimental solid-state, and SO-NEVPT2 calculated absorption spectra of 2-Cf averaged for both *cis* and *trans* geometries

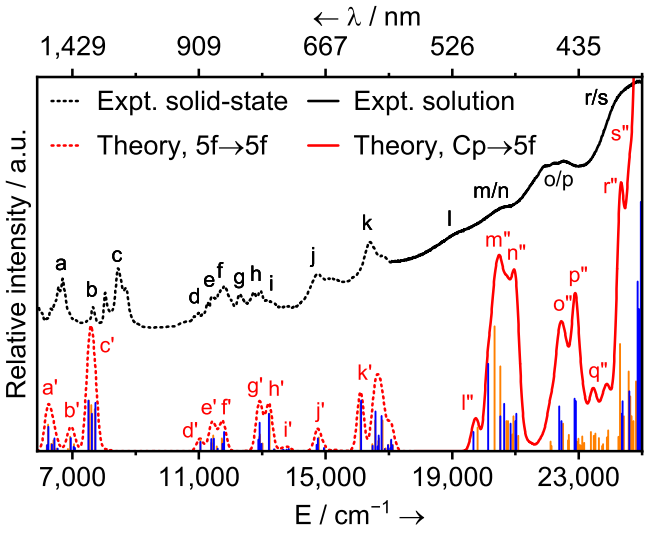

Experimental and SO-NEVPT2 calculated absorption spectra from the averaged results of both *cis*- and *trans*-**2-Cf** at the experimental geometries. Calculated 5f→5f absorption spectrum (red dashed line); calculated ligand→5f absorption spectrum (red solid line). The main absorption peaks are labelled by x (x = a – s), x′ (x = a – k) and x″ (x = l – s) for experimental, and theoretical 5f→5f, and ligand→5f transitions, respectively. The calculated intensity of Laporte-forbidden 5f→5f transitions (red dashed line) are too low to be visible and so were enlarged by ~57 times relative to that of ligand→5f (red solid line). Blue and orange bars represent the energy and oscillator strength for the calculated spectra of *cis*- and *trans*-[Cf(Cp^{tet})$_2$$Cl_2$K] complexes, respectively. The calculated spectrum was red-shifted by 1,543 cm^{-1} to align with the experimental absorption peaks at 14,766 cm^{-1} labelled j. See Supplementary Table 10.

Time-dependent DFT (TDDFT/PBE0) calculations were used to provide insight into differences between dark orange **2-Cf** and colourless **2-Dy** (Supplementary Figs. 69 – 70). For **2-Cf**, intense ligand→5f absorption features above *ca*. 18,000 cm^{-1} are consistent between *ab initio* calculations and experiment. In **2-Dy**, the lowest energy ligand→Dy 4f transitions occur at 39,653 and 40,385 cm^{-1} – this is more than 10,000 cm^{-1} higher in energy than for **2-Cf** (Supplementary Tables 14 – 15). The Cf 6d and Dy 5d orbitals in **2-Cf** and **2-Dy** have similar, albeit small, mixing with ligand orbitals as the d-orbitals are comparatively high in energy. The Cf 5f contribution to MOs is greater than Dy 4f (Supplementary Table 19). Hence, both UV-vis-NIR spectra and MO compositions validate the closer energetic proximity of ligand and metal f-orbitals in **2-Cf**

than that in **2-Dy**. This results in lower energy ligand→f transitions in **2-Cf**, and greater mixing between metal f-orbitals and ligand orbitals for Cf than Dy.

Conclusions

The structural characterization of **2–Cf** comes more than 70 years after the discovery of californium by Seaborg *et al.*, and 50 years since the first organocalifornium complex was proposed and characterized.[22] The Cf–C bond in **2-Cf** is polarized and largely ionic in nature. Energetic mismatch between the contracted Cf^{3+} 5f-orbitals, and C 2p-orbitals, is too large for significant covalent bonding, and the 6d manifold is largely energetically inaccessible. However, the substantially smaller energy gap between ligand- and f-orbitals in **2-Cf** *vs* those in the isoelectronic Dy analogue rationalizes the unusual orange colour of **2-Cf** – where ligand to metal charge transfer occurs in the visible range for Cf and far into the UV for Dy. These findings represent scarcely-studied subtle bonding and electronic changes at the frontier of isolable molecules in the periodic table.

Acknowledgements

We thank Dr. Iain May at Los Alamos National Laboratory (LANL) and Dr. Gregory P. Horne at Idaho National Laboratory for discussions. We acknowledge the U.S. Department of Energy (DOE), Office of Science (DOE-SC), Basic Energy Sciences (BES) Heavy Element Chemistry Program (HEC) at LANL (ERB, AJG, SAK, ZRJ, BLS, FDW, PY, JS; DE-AC52-06NA25396), at Florida State University (TEAS, ANG, JMS, CJW; DE-FG02-13ER16414), and at the University of California at Irvine (WJE, TFJ; DE-SC0004739). CAPG was sponsored by a Distinguished J. R. Oppenheimer Postdoctoral Fellowship (LANL-LDRD, 20180703PRD1). We thank LANL-LDRD (LMS, AJG; 20190091ER) for aspects of the ^{241}Am experimental work. Theoretical research was performed using EMSL (grid.436923.9), a DOE-SC User Facility sponsored by the Office of Biological and Environmental Research. JS also thanks the NSFC (22076130), and the Fundamental Research Funds for the Central Universities (20826041D4117) and start-up funds from Sichuan University. JNC and JDA acknowledges the U.S. Department of Energy, Office of Science, Isotope Development and Production for Research and Application subprogram within Office of Nuclear Physics for

^{241}Am sample conditioning and dispensing. JDA thanks the NNSA Plutonium Sustainment Program and the National Nuclear Security Administration (NNSA) Material Recycle and Recovery for funding. We thank Dr. Eva R. Birnbaum and Beverly L. Ortiz for procurement of ^{241}Am through the National Isotope Development Center, purchased with LANL DOE-SC-BES-HEC funds.

Author contributions

ERB, WJE, AJG, SAK, and PY devised the project. CAPG led lanthanide synthetic protocol development and performed Cf and Am synthetic work and characterization with AJG, with expertise and support from LMS and FDW (UV-vis-NIR), MTJ (NMR), TFJ (ligand preparation), BLS (single-crystal XRD), and SFB (radiological safety). SAK, NHA, and ZRJ prepared the LANL ^{249}Cf stock solution; ANG, JMS, and CJW prepared the FSU ^{249}Cf stock solution; LMS, AJG, MRJ, and JNC prepared the ^{241}Am stock at LANL. JCW provided supporting characterization of lanthanide compounds. JS, ERB, and PY performed and analysed all theoretical work. Principal manuscript writing was by CAPG, JS, AJG, SAK, WJE, ERB, and PY, with input and editing from all authors.

Competing interests

The authors declare no competing interests.

Data Availability Statement

The data that support the findings of this study are available within the paper and its supplementary information files.

Cambridge Crystallographic Data Centre (CCDC) deposition numbers are 2025245 (**1-^{241}Am**), 2058952 (**1-Ho**), 2025247 (**2-Cf**), 2025249 (**2-Gd$^{\alpha}$**), 2092534 (**2-Gd$^{\beta}$**), 2025248 (**2-Dy**), 2063323 (**3**) and 2025250 (**4**). These data can be obtained free of charge from the CCDC via www.ccdc.cam.ac.uk/data_request/cif.

References

Methods

Comprehensive Cf experimental details and photographs are provided in the Supplementary Information file. Here, we offer key methodology details abridged from the Supplementary Information regarding the synthesis of **2-Cf**, specifically, the central characterized molecule of this manuscript. The approach towards prior small-scale lanthanide development reactions was crucial in allowing the Cf experiment to be successful. We performed numerous small scale syntheses of $[Ln(Cp^{tet})_3]$ (Ln = Sm, **1-Sm**; Gd, **1-Gd**) and $[Ln(Cp^{tet})_2Cl_2K(OEt_2)]_n$ (Ln = Gd, **2-Gd**; Dy, **2-Dy**) to ensure that we had experimental conditions that would reliably deliver crystals suitable for single crystal X-ray diffraction, ideally within a single day from commencement of the reaction to obtaining the crystal structure to minimize radiolytic damage to the molecular product and single crystal quality. While the trivalent ionic radius of Cf is closer to Eu than to Sm (6-coordinate: Sm, 0.958 Å; Eu, 0.947 Å; Cf, 0.95 Å), the latter was used as an analogue in the synthesis of **1-Ln** because the ready accessibility of divalent Eu invariably led to reduction when $EuCl_3$ has been used with KCp^{tet} in our hands. The 6-coordinate trivalent ionic radius of Gd (0.938 Å) is smaller than that of Cf and thus serves to check for differences in chemistry due to errors in the reported ionic radius of Cf. These Ln small-scale optimized protocol details are provided in the Supplementary Information.

Preparation '$CfCl_3(DME)_n$': In a 20 mL glass scintillation vial, a pale green aqueous (6 M HCl) solution containing 2.0 mg $^{249}Cf^{3+}$ as a chloride complex, was reduced to dryness under a flow of argon gas at room temperature. The mint green residue was then placed *in vacuo* in the antechamber of a helium-atmosphere negative pressure transuranium glovebox for 12 hours. The next day, DME (2 mL) was added followed by stirring for 2 minutes which resulted in a pale green suspension and a colourless solution. Solids were freed from the glass with a spatula which was rinsed with DME (~0.1 mL). The suspension was heated to 50 °C for 10 minutes without any appreciable further dissolution being observed. After cooling to ambient temperature, Me_3SiCl (1.5 mL) was added dropwise with stirring then heated to 50 °C for 2 hours. After cooling to ambient temperature caused more solids to precipitate. Hexanes (3 mL) was added to the off-white/pale-green suspension with stirring for 10 minutes. This resulted in a colourless solution with pale green solids. The suspension was stored at −35 °C for 20 minutes to help the solids to settle to the bottom of the vial. The

colourless supernatant was pipetted away and the solid stirred with hexanes (3 mL). After settling again at −35 °C, the colourless hexane was pipetted away; and this procedure was repeated once more. The solid was dried *in vacuo* for 30 minutes, to afford a mint green powder. The solid was stirred with Et_2O (2 mL) for 15 minutes, then hexane (3 mL) was added. The mixture was allowed to settle at −35 °C. After removing the colourless supernatant using a pipette, the solids were dried *in vacuo* for 2 hours to afford putative '$CfCl_3(DME)_n$' as a mint green powder that was used immediately.

Synthesis of $[Cf(Cp^{tet})_2Cl_2K(OEt_2)]_n$ *(2-Cf):* KCp^{tet} (4.5 mg, 30 μmol, 3.5 equiv.) was added to the solid $CfCl_3(DME)_n$ residue prepared above, in the same 20 mL scintillation vial used for the prior step. The vial containing KCp^{tet} was rinsed with Et_2O (2 mL) into the reaction vial. The colour immediately changed to pale orange/pinkish, and was stirred at room temperature for 90 minutes, during this time the colour changed from pinkish, to salmon-orange, and finally to orange-yellow. The yellow solution was filtered from pale solids through 2 half-discs of glass microfiber mounted in a glass pipette, into a 4 mL glass vial. The reaction vial and filter discs were washed with Et_2O (1 mL) until the solution came through colourless. The supernatant was concentrated to 0.5 mL *in vacuo* which caused some oily dark material to adhere to the sides of the vial, additional Et_2O (~0.1 mL) was added and this material was warmed into solution by sealing the vial lid and warming on a hotplate set to 80 °C which caused complete dissolution after 1 minute. The hotplate was allowed to cool to room temperature undisturbed over 45 minutes with the vial left on it. A modest crop of dark orange crystals to formed, and this was dried to an orange power *in vacuo*. The supernatant was transferred to a fresh 4 mL glass vial and stored in the glovebox freezer (−35 °C) overnight but this did not yield any further crystals.

1 Mingos, M. & Crabtree, R. *Comprehensive organometallic chemistry III*. (Elsevier Science, 2007).

2 Zalkin, A. & Raymond, K. N. Structure of di-π-cyclooctatetraeneuranium (Uranocene). *J. Am. Chem. Soc.* **91**, 5667-5668, doi:https://doi.org/10.1021/ja01048a055 (1969).

3 Kealy, T. J. & Pauson, P. L. A New Type of Organo-Iron Compound. *Nature* **168**, 1039-1040, doi:10.1038/1681039b0 (1951).

4 Hartline, D. R. & Meyer, K. From Chemical Curiosities and Trophy Molecules to Uranium-Based Catalysis: Developments for Uranium Catalysis as a New Facet in Molecular Uranium Chemistry. *JACS Au* **1**, 698-709, doi:https://doi.org/10.1021/jacsau.1c00082 (2021).

5 Pagano, J. K. *et al.* Actinide 2-metallabiphenylenes that satisfy Hückel's rule. *Nature* **578**, 563-567, doi:https://doi.org/10.1038/s41586-020-2004-7 (2020).

6 Apostolidis, C., Dutkiewicz, M. S., Kovács, A. & Walter, O. Solid-State Structure of Tris-Cyclopentadienide Uranium(III) and Plutonium(III). *Chem. Eur. J.* **24**, 2841-2844, doi:10.1002/chem.201704845 (2018).

7 Windorff, C. J. *et al.* Identification of the Formal +2 Oxidation State of Plutonium: Synthesis and Characterization of $\{Pu^{II}[C_5H_3(SiMe_3)_2]_3\}^-$. *J. Am. Chem. Soc.* **139**, 3970-3973, doi:https://doi.org/10.1021/jacs.7b00706 (2017).

8 Formanuik, A. *et al.* Actinide covalency measured by pulsed electron paramagnetic resonance spectroscopy. *Nat. Chem.* **9**, 578-583, doi:https://doi.org/10.1038/nchem.2692 (2017).

9 Dutkiewicz, M. S., Apostolidis, C., Walter, O. & Arnold, P. L. Reduction chemistry of neptunium cyclopentadienide complexes: from structure to understanding. *Chem. Sci.* **8**, 2553-2561, doi:10.1039/C7SC00034K (2017).

10 Apostolidis, C. *et al.* A Structurally Characterized Organometallic Plutonium(IV) Complex. *Angew. Chem., Int. Ed.* **56**, 5066-5070, doi:https://doi.org/10.1002/anie.201701858 (2017).

11 Dutkiewicz, M. S. *et al.* Organometallic neptunium(III) complexes. *Nat. Chem.* **8**, 797-802, doi:https://doi.org/10.1038/nchem.2520 (2016).

12 Liddle, S. T. The Renaissance of Non-Aqueous Uranium Chemistry. *Angew. Chem., Int. Ed.* **54**, 8604-8641, doi:https://doi.org/10.1002/anie.201412168 (2015).

13 Goodwin, C. A. P. *et al.* $[Am(C_5Me_4H)_3]$: An Organometallic Americium Complex. *Angew. Chem., Int. Ed.* **58**, 11695-11699, doi:https://doi.org/10.1002/anie.201905225 (2019).

14 Sonnenberger, D. C. & Gaudiello, J. Synthesis and cyclic voltammetric study of bis(pentamethylcyclopentadienyl)neptunium dichloride. *J. Less-Common. Met.* **126**, 411-414, doi:https://doi.org/10.1016/0022-5088(86)90350-4 (1986).

15 Laubereau, P. G. The formation of dicyclopentadienylberkeliumchloride. *Inorg. Nucl. Chem. Lett.* **6**, 611-616, doi:https://doi.org/10.1016/0020-1650(70)80057-5 (1970).

16 Cary, S. K. *et al.* A series of dithiocarbamates for americium, curium, and californium. *Dalton Trans.* **47**, 14452-14461, doi:http://doi.org/10.1039/C8DT02658K (2018).

17 Polinski, M. J. *et al.* Unusual structure, bonding and properties in a californium borate. *Nat. Chem.* **6**, 387-392, doi:http://doi.org/10.1038/nchem.1896 (2014).

18 Sykora, R. E., Assefa, Z., Haire, R. G. & Albrecht-Schmitt, T. E. First Structural Determination of a Trivalent Californium Compound with Oxygen Coordination. *Inorg. Chem.* **45**, 475-477, doi:10.1021/ic051667v (2006).

19 Carnall, W. T. A systematic analysis of the spectra of trivalent actinide chlorides in D_{3h} site symmetry. *J. Chem. Phys.* **96**, 8713-8726, doi:https://doi.org/10.1063/1.462278 (1992).

20 Carnall, W. T., Fried, S. & Wagner, F. Absorption spectrum of $CfCl_3$. *J. Chem. Phys.* **58**, 1938-1949, doi:https://doi.org/10.1063/1.1679455 (1973).

21 Burns, J. H., Peterson, J. R. & Baybarz, R. D. Hexagonal and orthorhombic crystal structures of californium trichloride. *J. Inorg. Nucl. Chem.* **35**, 1171-1177, doi:https://doi.org/10.1016/0022-1902(73)80189-7 (1973).

22 Laubereau, P. G. & Burns, J. H. Microchemical preparation of tricyclopentadienyl compounds of berkelium, californium, and some lanthanide elements. *Inorg. Chem.* **9**, 1091-1095, doi:http://doi.org/10.1021/ic50087a018 (1970).

23 Streitwieser, A. & Mueller-Westerhoff, U. Bis(cyclooctatetraenyl)uranium (uranocene). A new class of sandwich complexes that utilize atomic f orbitals. *J. Am. Chem. Soc.* **90**, 7364-7364, doi:https://doi.org/10.1021/ja01028a044 (1968).

24 Minasian, S. G. *et al.* New evidence for 5f covalency in actinocenes determined from carbon K-edge XAS and electronic structure theory. *Chem. Sci.* **5**, 351-359, doi:https://doi.org/10.1039/C3SC52030G (2014).

25 Evans, W. J. Tutorial on the Role of Cyclopentadienyl Ligands in the Discovery of Molecular Complexes of the Rare-Earth and Actinide Metals in New Oxidation States. *Organometallics* **35**, 3088-3100, doi:10.1021/acs.organomet.6b00466 (2016).

26 Hayton, T. W. Recent developments in actinide-ligand multiple bonding. *Chem. Commun.* **49**, 2956-2973, doi:https://doi.org/10.1039/C3CC39053E (2013).

27 Jones, M. B. & Gaunt, A. J. Recent developments in synthesis and structural chemistry of nonaqueous actinide complexes. *Chem. Rev.* **113**, 1137-1198, doi:https://doi.org/10.1021/cr300198m (2013).

28 Baumgärtner, F., Fischer, E. O., Kanellakopulos, B. & Laubereau, P. Tri(cyclopentadienyl)americium(III). *Angew. Chem., Int. Ed.* **5**, 134-135, doi:https://doi.org/10.1002/anie.196601342 (1966).

29 Laubereau, P. G. & Burns, J. H. Tricyclopentadienyl-curium. *Inorg. Nucl. Chem. Lett.* **6**, 59-63, doi:https://doi.org/10.1016/0020-1650(70)80285-9 (1970).

30 Kirker, I. & Kaltsoyannis, N. Does covalency *really* increase across the 5f series? A comparison of molecular orbital, natural population, spin and electron density analyses of $AnCp_3$ (An = Th-Cm; Cp = η^5-C_5H_5). *Dalton Trans.* **40**, 124-131, doi:https://doi.org/10.1039/C0DT01018A (2011).

31 Strittmatter, R. J. & Bursten, B. E. Bonding in tris(η^5-cyclopentadienyl) actinide complexes. 5. A comparison of the bonding in neptunium, plutonium, and transplutonium compounds with that in lanthanide compounds and a transition-metal analog. *J. Am. Chem. Soc.* **113**, 552-559, doi:https://doi.org/10.1021/ja00002a024 (1991).

32 Kozimor, S. A. *et al.* Trends in covalency for d- and f-element metallocene dichlorides identified using chlorine K-edge X-ray absorption spectroscopy and time-dependent density functional theory. *J. Am. Chem. Soc.* **131**, 12125-12136, doi:https://doi.org/10.1021/ja9015759 (2009).

33 Arney, D. S. J. & Burns, C. J. Synthesis and Properties of High-Valent Organouranium Complexes Containing Terminal Organoimido and Oxo Functional Groups. A New Class of Organo-f-Element Complexes. *J. Am. Chem. Soc.* **117**, 9448-9460, doi:https://doi.org/10.1021/ja00142a011 (1995).

34 Apostolidis, C. *et al.* $[An(H_2O)_9](CF_3SO_3)_3$ (An=U-Cm, Cf): Exploring Their Stability, Structural Chemistry, and Magnetic Behavior by Experiment and Theory. *Angew. Chem., Int. Ed.* **49**, 6343-6347, doi:https://doi.org/10.1002/anie.201001077 (2010).

35 Polinski, M. J. *et al.* Chirality and Polarity in the f-Block Borates $M_4[B_{16}O_{26}(OH)_4(H_2O)_3Cl_4]$ (M=Sm, Eu, Gd, Pu, Am, Cm, and Cf). *Chem. Eur. J.* **20**, 9892-9896, doi:https://doi.org/10.1002/chem.201403820 (2014).

36 Cary, S. K. *et al.* Emergence of californium as the second transitional element in the actinide series. *Nat. Commun.* **6**, doi:http://doi.org/10.1038/ncomms7827 (2015).

37 Galley, S. S. *et al.* Synthesis and Characterization of Tris-chelate Complexes for Understanding *f*-Orbital Bonding in Later Actinides. *J. Am. Chem. Soc.* **141**, 2356-2366, doi:https://doi.org/10.1021/jacs.8b10251 (2019).

38 Shannon, R. D. Revised effective ionic radii and systematic studies of interatomic distances in halides and chalcogenides. *Acta Crystallogr. A* **32**, 751-767, doi:10.1107/s0567739476001551 (1976).

39 Schumann, H., Glanz, M., Hemling, H. & Ekkehard Hahn, F. Metallorganische Verbindungen der Lanthanoide. 93 [1]. Tetramethylcyclopentadienyl-Komplexe ausgewählter 4f-Elemente. *Z. Anorg. Allg. Chem.* **621**, 341-345, doi:https://doi.org/10.1002/zaac.19956210302 (1995).

40 Jenkins, T. F. *et al.* Tetramethylcyclopentadienyl Ligands Allow Isolation of Ln(II) Ions across the Lanthanide Series in [K(2.2.2-cryptand)][$(C_5Me_4H)_3Ln$] Complexes. *Organometallics* **37**, 3863-3873, doi:10.1021/acs.organomet.8b00557 (2018).